The 5th European sCO_2 Conference for Energy Systems
March 14-16, 2023, Prague, Czech Republic

2023-sCO2.eu-131

THE STEADY BEHAVIOR OF THE SUPERCRITICAL CARBON DIOXIDE NATURAL CIRCULATION LOOP

Marko Draskic
Process & Energy - 3mE
Delft University of Technology
Delft, The Netherlands
m.draskic@tudelft.nl

Benjamin Bugeat
Process & Energy - 3mE
Delft University of Technology
Delft, The Netherlands

Rene Pecnik*
Process & Energy - 3mE
Delft University of Technology
Delft, The Netherlands
r.pecnik@tudelft.nl

ABSTRACT

The steady state behavior of thermodynamically supercritical natural circulation loops (NCLs) is investigated in this work. Experimental steady state results with supercritical carbon dioxide are presented for reduced pressures in the range of 1.1-1.5, and temperatures in the range of 20-65 °C. Distinct thermodynamic states are reached by traversing a set of isochors. A generalized equation for the prediction of the steady state is presented, and its performance is assessed using empirical data. Changes of mass flow rate as a result of changes of thermodynamic state, heating- and driving height are shown to be accurately captured by the proposed predictive equation. However, the enhanced viscous losses in the instrumentation of the loop and in the proximity of heat transfer equipment are shown to significantly limit the steady state flow rate. Subsequently, the findings are put forward in aid of the development of safe, novel supercritical natural circulation facilities.

INTRODUCTION

When a flow loop is heated at one of its vertical legs and cooled at the other, a natural convection is induced. The flow- and cooling rates of single phase natural circulation facilities are generally orders of magnitude too small to serve any purpose in industrial applications. However, if the operating fluid is in a thermodynamically supercritical state, considerable flow rates can be obtained due to strong density variations in the vicinity of the critical point. The flow rates generated with these simple systems can be used in settings in which an elsewise moderate flowrate is required, but where problems stemming from leakages, power outages and mechanical noise associated with forced convective flows need to be avoided. As such, supercritical fluid NCLs can act as reliable, off-grid cooling solutions for nuclear reactors, in case large heat sinks are present. Additionally, these systems can be used for the passive removal of heat from solar heater assemblies, or for the generation of steady, pulseless flows for sensitive experiments. However, as the properties of supercritical media vary greatly with state, the prediction of the steady state of supercritical NCLs for their potential implementation is not straightforward.

The steady state of supercritical natural circulation loops has previously been investigated using both numerical and experimental approaches. In the numerical literature, a one-dimensional transient model is most commonly used to predict both the steady and unsteady behavior of the considered loops [1]–[4], although three-dimensional approaches have also been undertaken [5]. The mass flow rate of a natural convection loop has been predicted to attain a maximum with varying heating rates [1], [2]. Furthermore, a rise in mass flow rate is expected with increasing loop heights, and increasing channel diameters [1], [3], [5]. On the contrary, an increase of the loop length is expected to have a limiting effect on the flow rate of the loop [5] The influence of thermodynamic state on the steady behavior of supercritical NCLs is briefly touched upon in [4]. Here, increases in both the filling mass and the heating rate are predicted to result in an increase in loop pressure and subsequently loop flow rate for the range of considered parameters. Similar conclusions can be drawn from experimental investigations of NCLs with supercritical media. An increase in mass flow rate with increasing heating rate was first measured by Tokanai et al., [6]. The broader range of results presented in Liu et al. [7] also show the previously discussed maximum in the mass flow rate with increasing heating. As predicted, an increase in system temperature yields an increase in static pressure at a set charge [8], [9], and an increase in mass flow rate for the considered parameters in the work of Sadhu et al., as shown in [9].

The above findings only consider and discuss an NCL's sensitivity to changes in specific parameters. A generalized consideration of all variables that affect the steady state is however needed in aid of the reliable design of future facilities. A first correlation of the flow rate of a liquid-like supercritical carbon dioxide NCL, in terms of Grashof and Prantl numbers, was presented by Yoshikawa et al., [10]. A more elaborate approach was put forward by Swapnalee at al. [11], following the modus operandi of Vijayan et al. for single-phase fluids [12], [13]. Here, an expression for the mass flow rate is derived from the one-dimensional steady state momentum equation. In order to characterize the distribution of density in the equation

* corresponding author

DOI: 10.17185/duepublico/77307

that follows, the change in loop density has to be expressed as a function of the change in enthalpy in the heater. For this, the relationship between dimensionless density and dimensionless enthalpy introduced by Ambrosini et al. [14] is used. Here, the adequate overlap of the dimensionless quantities for a broad range of supercritical pressures makes that a single curve can be used to express the relationship between density and enthalpy. Swapnalee et al. [11] use three distinct linear fits of the constitutive curve to express an expected change of density for three separate ranges of subcooling. From this, a straightforward equation for the NCL flow rate follows, which can be expressed in terms of a pipe diameter based Grashof (Gr_D) and a Reynolds (Re_D) number. A very similar approach is followed in the work of Liu et al. [15], where a two-region linear fit of Ambrosini's[14] curve is used to derive an expression for the steady mass flow rate. As the true evolution with state is however continuous, the chosen discrete description of thermodynamic properties is expected to introduce significant errors in the prediction of the flow rate. Additionally, the absence of the characterization of experimental loop minor losses in both works makes that the found relationship between Gr_D and Re_D is configuration specific. As the driving forces are generally limited in comparison with forced convective systems, setup-specific pressure losses in equipment can be expected to have a considerable effect on the flow rates of NCLs.

In this work, a revised generalized equation for the prediction of the steady flow rate of natural circulation loops with supercritical media is proposed. Consequently, the generalized formula is assessed using the experimental results of a new supercritical carbon dioxide natural circulation facility at the Process & Energy laboratory of the Delft University of Technology. In order to find the causes for possible disagreement between theory and experiment, the contributions of state, heating rate, configuration and pressure losses are independently considered.

GENERALIZED FLOW EQUATION

Away from regions with considerable radial temperature gradients, the flow in a NCL is expected to display behavior similar to that of a developed pipe flow. As such, a generalized equation is sought from the mass- and momentum balance of a one-dimensional flow. Here, a constant-area pipe, and negligible viscous heating are assumed. A geometry that can be described with figure 1 is considered. Here, a heater and a cooler are consecutively placed along a closed flow loop. In the figure, the heater and cooler are indicated with red and blue circles, respectively.

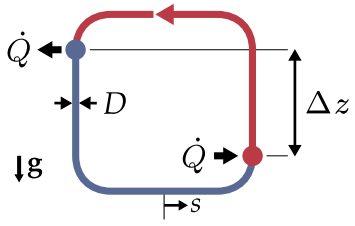

Figure 1: Schematic of simplified NCL. Low- and high density sections indicated in red and blue, respectively. Preferential flow direction indicated with red arrow.

The mass- and momentum balance equations for the considered system are described as a function of streamwise coordinate s:

$$\frac{1}{A_{\mathrm{cs}}}\frac{\mathrm{d}}{\mathrm{d}s}(\dot{m}) = 0, \tag{1}$$

$$\frac{\mathrm{d}}{\mathrm{d}s}\left(\frac{1}{A_{\mathrm{cs}}^2}\frac{\dot{m}^2}{\rho} + P\right) = \gamma\rho g - \frac{2f}{D}\frac{1}{A_{\mathrm{cs}}^2}\frac{\dot{m}^2}{\rho}. \tag{2}$$

Here, the coefficient $\gamma(s) \in [-1, 1]$ is used to account for the direction of gravity with respect to the flow at coordinate s. The rightmost term in equation (2) serves to describe viscous losses in the system, using dimensionless Fanning factor f. Given that the mass flow rate $\dot{m}$ is a constant, and that $\oint \mathrm{d}(1/\rho)$ and $\oint \mathrm{d}P$ are zero for a closed loop, the path integral of equation (2) reduces to

$$\oint \rho g \,\mathrm{d}s = \frac{2}{DA_{\mathrm{cs}}^2}\oint \frac{f\dot{m}^2}{\rho}\,\mathrm{d}s. \tag{3}$$

A force balance with only contributions from the driving buoyancy distribution and viscous losses in the loop remains. The system is ultimately driven by the density difference $\Delta\rho$ over the vertical section between the cooler and heater with equivalent length Δz. Here, Δz is the vertical distance between the cooler and the heater, if they were to be modeled as point sources and point sinks for heat transfer. In reality, a vertical distribution of ρ is found in both heat exchangers. As such, Δz depends on the heat transfer mode- and rate, and will attain a value close to the vertical centerline distance. Given the above, equation (3) can be rewritten to

$$\Delta\rho g \Delta z A_{\mathrm{cs}} = \frac{1}{L}\frac{A_{\mathrm{p}}}{A_{\mathrm{cs}}^2}\frac{\dot{m}^2}{2\rho_{\mathrm{m}}}\sum_{i=1}^{n}(f_{\mathrm{i}}L_{\mathrm{i}}). \tag{4}$$

Here, the viscous loss contributions of all sections i are to be summed. By linearizing the change in density with varying enthalpy at the mean loop temperature $T_{\mathrm{m}} = 1/L\int T(s)\mathrm{d}s$ and mean loop pressure P_{m}, and assuming constant pressure in the heat transfer equipment, $\Delta\rho$ can be expressed as a function of a change in enthalpy Δh:

$$\left.\frac{\partial\rho}{\partial h}\right|_p \Delta h g \Delta z A_{\mathrm{cs}} = \frac{A_{\mathrm{p}}}{A_{\mathrm{cs}}^2}\frac{\dot{m}^2}{2\rho_{\mathrm{m}}}\frac{\Sigma\left(f_{\mathrm{i}}L_{\mathrm{i}}\right)}{L}. \tag{5}$$

Using the chain rule, the thermodynamic quantity $\partial\rho/\partial h|_p$ can be rewritten to $\rho_{\mathrm{m}}\beta_{\mathrm{m}}/c_{\mathrm{p,m}}$. Here, all thermodynamic quantities are to be evaluated at T_{m}. Lastly, given that $\Delta h = \dot{Q}/\dot{m}$, $A_{\mathrm{cs}} = \pi D^2/4$ and $A_{\mathrm{p}} = \pi DL$ an equation as a function of design parameters of a supercritical fluid NCL follows:

$$\dot{m}^3 = \frac{\pi^2 g}{32}\cdot\underbrace{\frac{\rho_{\mathrm{m}}^2\beta_{\mathrm{m}}}{c_{\mathrm{p,m}}}}_{\text{Fluid properties}}\cdot\underbrace{\dot{Q}\Delta z D^5}_{\text{Configuration}}\cdot\underbrace{\frac{1}{\Sigma(f_{\mathrm{i}}L_{\mathrm{i}})}}_{\text{Viscous losses}}. \tag{6}$$

Equation (6) expresses expected mass flow rate $\dot{m}$ as a function of a state dependent group of variables, a configuration and geometry specific group, and a viscous loss term. The viscous loss term $\Sigma(f_{\mathrm{i}}L_{\mathrm{i}})$ accounts for both viscous losses in developed sections, and for additional losses in loop equipment and bends. Equation (6) has to be solved for iteratively, since the viscous loss term is a function of mass flow rate $\dot{m}$. Furthermore, as the Reynolds numbers for the warm and the cold leg of the system

DOI: 10.17185/duepublico/77307

differ at constant $\dot{m}$, their viscous losses have to be solved for independently. The fluid properties of the respective sections can be solved for at $h_{\mathrm{h,c}} = h_{\mathrm{m}} \pm \frac{1}{2}\Delta h|_P$, the value of which follows from the guess for $\dot{m}$.

In order to allow for ease of experimental fitting, equation (6) should be rewritten in dimensionless form. For this purpose, dimensionless quantities Gr_{D} and Re_{D} are introduced:

$$Gr_{\mathrm{D}} = \frac{\rho_{\mathrm{m}}^2 \beta_{\mathrm{m}}}{c_{\mathrm{p,m}} \mu_{\mathrm{m}}^2} \frac{\dot{Q} g D^3}{\dot{m}}, \quad Re_{\mathrm{D}} = \frac{\rho_{\mathrm{m}} U D}{\mu_{\mathrm{m}}}. \tag{7}$$

Consequently, the Grashof number can be expressed as a function of the Reynolds number:

$$Gr_{\mathrm{D}} = 2\frac{\Sigma(f_{\mathrm{i}} L_{\mathrm{i}})}{\Delta z} \cdot Re_{\mathrm{D}}^2. \tag{8}$$

In case the pressure losses in loop equipment attain negligible magnitudes, and a fanning factor expression of the form $f = p/Re_{\mathrm{D}}^b$ is used, equation (8) reduces to

$$Re_{\mathrm{D}} = \left(\frac{\Delta z}{2pL} \cdot Gr_{\mathrm{D}} \right)^{\frac{1}{2-b}}. \tag{9}$$

EXPERIMENTAL FACILITY & METHODOLOGY

The experimental facility designed for- and used in this work is depicted schematically in figure 2. As the heater and cooler are located along the vertical legs of the system, a preferential flow direction prevails. For steady flows, a counter-clockwise circulation is expected in the perspective of the figure. The dimensions of the flow loop and the range of conditions within which it has been designed to operate are specified in table 1. Whereas most of the system is joined using detachable stainless steel tube fittings, EPDM or PTFE is used in components where non-metallic soft seals are required [16]. Heat is supplied to the system using a series of movable electric band heaters. In order to minimize heat losses to the surroundings, the circulation loop is insulated with a 40 mm thick annulus of rockwool. The loop is cooled using a tube-in-tube counter-current heat exchanger. Here, the outer annulus is equipped with baffles to aid in the distribution of the coolant. The inlet temperature of the cooler is controlled using a Julabo FP51-SL refrigerated circulator. Whilst mostly simplistic of nature, the loop is also equipped with flow- and state control devices. An adjustable local pressure loss is introduced using a regulating needle valve. Additionally, the volume in the loop can be varied using a 1 l piston accumulator, indicated below ⑤ in the figure. Here, nitrogen is used as the secondary medium.

Parameter & Description		Value/Range	Unit
H	Loop height	4.0	m
L	Loop length	10.0	m
D	Inside diameter	21.1	mm
Δz	Driving height	≤ 2.5	m
P	Design pressure	≤ 140	bar
T	Design temperature	$-20 \leq T \leq 65$	°C

Table 1: Test loop description

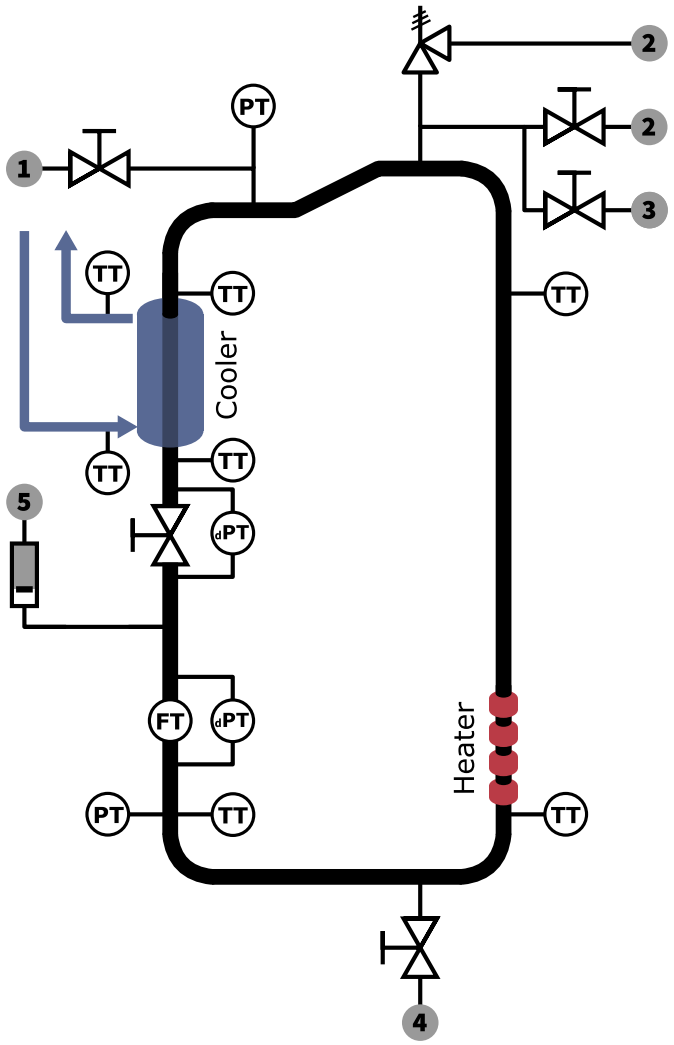

Figure 2: Schematic depiction of the TU Delft Process & Energy sCO_2 natural circulation loop. As indicated in grey, the system is connected to ① a CO_2 bottle with dip tube, ② a CO_2 purge that is connected to the lab's gas vent system, ③ a vacuum pump, ④ a drain, and ⑤ a nitrogen bottle. The electric heater and annular cooler are indicated in red and blue, respectively.

The facility is equipped with a series of transmitters for the continuous monitoring of its performance. Bulk temperatures are measured using PT100 resistance thermometers with a nominal accuracy of $\pm 0.1\ ^{\circ}C$, which are laterally inserted into the flow. Absolute pressure measurements are taken using welded STS ATM.1st transmitters, with a nominal uncertainty of ± 0.16 bar or 0.1%. Furthermore, the loop includes a Rheonik RHM08 Coriolis mass flow meter with a nominal uncertainty of 0.2%. Finally, two Siemens SITRANS P420 differential pressure sensors were used for the quantification of the viscous losses in both the Coriolis meter and the regulating valve. The transducer data are acquired at 1Hz using a NI cRIO-9074, with RTD module NI-9216, analog in- (NI-9208) and output (NI-9266) modules, and digital input module NI-9421. A Labview user-interface for the real-time visualization of the data was developed to complement the data acquisition structure. Here, the interpolation of tabulated thermodynamic properties allows for the live monitoring of various compound quantities.

DOI: 10.17185/duepublico/77307

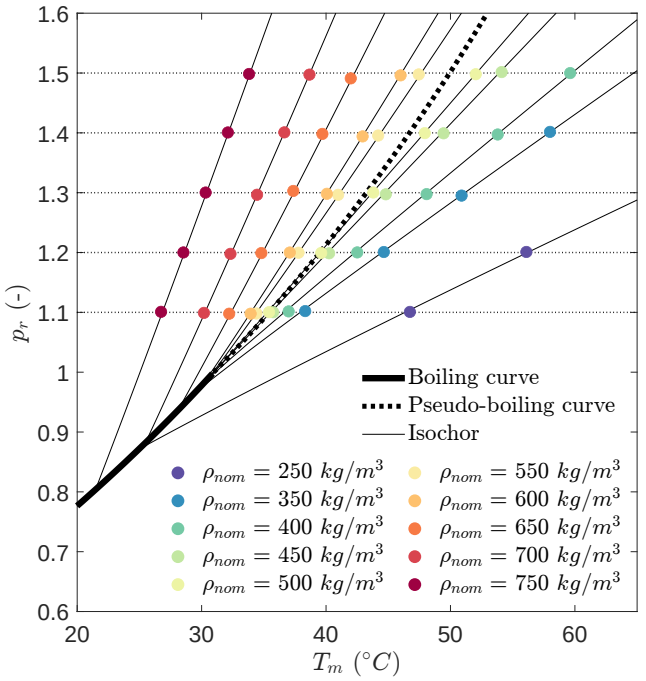

Figure 3: Lines of constant mass at set system volume for carbon dioxide at supercritical pressure. Current experimental data points indicated at measured T_m and P_m for all considered nominal densities. Boiling- and pseudo-boiling curves indicated with thick solid and dashed lines, respectively

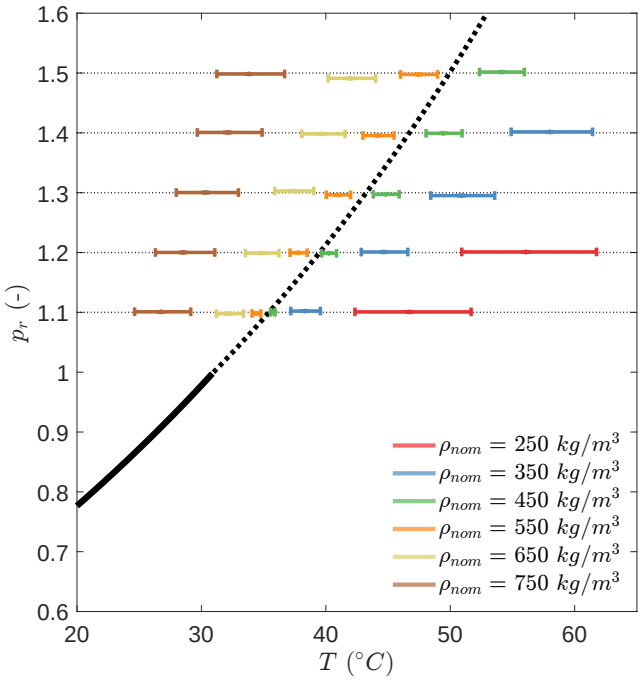

Figure 4: System temperature ranges for selected loop filling masses, at $\dot{Q} = 800$ W, $\Delta z = 2.5$ m. Range is bound by greatest and lowest measured temperature in the loop. Boiling- and pseudo-boiling curves indicated with solid and dashed lines, respectively.

In order to fill the loop, the system is first brought to moderate pressures. Consequently, a blow-off valve at the top of the loop is used to purge the system of non-condensable gases. Additionally, a valve at the bottom of the loop is opened to drain the loop of unwanted liquids. After evacuating the system with a vacuum pump, liquid carbon dioxide of a high purity is fed to the system from a cylinder with a dip tube. As the bottle is weighed, the filling mass of the loop is known. Once an equilibrium in pressure is reached between the bottle and the experimental facility, the loop is cooled. As a result, the loop pressure decreases to below the vapor pressure of the bottle, resulting in a flow of carbon dioxide towards the facility. By moderately heating the loop during this cooling step, a natural flow is generated that allows for greater cooling rates, and therewith accelerates the filling process.

In this work, the thermodynamic space is explored by traversing a set of isochors. As shown in figure 3, a desired supercritical pressure can be attained for different filling masses at different loop temperatures. During operation, the coolant temperature is adjusted at a constant volume to attain the appropriate pressure. As such, a constant mean state can be maintained for varying heating rates. The mean state is both continuously and a posteriori evaluated by assuming a linear distribution of T in the heat transfer equipment. The range of states that was therewith reached in this work is listed in table 2, and depicted in figure 3. The distinct thermodynamic states were attained for heating rates of both $400\ W$ and $800\ W$, and are used in discussions of the dependency on thermodynamic state of the mass flow rate and the assessment of the performance of the generalized equation.

Parameter & Description		Value/Range	Unit
$\dot{Q}$	Heating rate	≤ 2	kW
ρ_m	Mass density	$250 \leq \rho_\mathrm{m} \leq 750$	kg m^{-3}
$\mathrm{P_m}$	Operating pressure	$81 \leq \mathrm{P_m} \leq 111$	bar
$\mathrm{T_m}$	Operating temperature	$20 \leq \mathrm{T_m} \leq 60$	°C

Table 2: Operating range

RESULTS & DISCUSSION

During the steady operation of the natural circulation loop, the loop temperature distribution varies with thermodynamic state. The loop temperature distribution for an assortment of states within the considered range is depicted in figure 4. The natural flow is driven by moderate temperature gradients, especially in the vicinity of the pseudo-critical line. With increasing pressure beyond the critical point, the pseudo-critical curve gradually transforms from a point of near-discrete phase transition to a gradually increasing region of mild property gradients. Additionally, as the fluid's specific heat near this curve decreases with pressure, less variation of driving temperature is found along isobars of greater magnitudes. Of course, a quantitative assessment of the loop temperature distribution follows from the steady state mass flow rate. If the loop mass flow rate is known, the loop temperature maxima and minima can be obtained using $T_\mathrm{max,min} = T_\mathrm{m} \pm \dot{Q}/(2\dot{m}c_\mathrm{p,m})$. Using the experimental mass flow rate $\dot{m}_\mathrm{exp}$, close agreement with experimental data is found for the considered range of thermodynamic states.

In this work, equation (9) is proposed for the prediction of steady mass flow rate $\dot{m}$. A comparison of equation (9) with experimental data is given in figure 5. Here, no minor pressure

DOI: 10.17185/duepublico/77307

losses are considered in determining the viscous loss term of equation (9), consistent with previous approaches in existing literature. As the value of Re_D for all current empirical data exceeds 10^4, Blasius viscous loss constants for hydrodynamically smooth turbulent pipe flow $p = 0.25$ and $b = 0.0791$ are used. The experimental data for this figure is obtained in the absence of the regulating valve depicted in figure 2. The current prediction is expected to yield values of comparable magnitude as the generalized formulae of Swapnalee and Liu [11], [15], as similar approaches are undertaken. As shown in figure 5, significantly lower empirical Reynolds numbers were however obtained in the current experiments. Disagreement of the dimensionless quantities of a similar extent was also found in the work of Sadhu et al., [9]. In search of generality, an attempt is made to find the source of disparity between the prediction and the found experimental data. Hence, the contributions of the individual terms in dimensional equation (6) are further investigated.

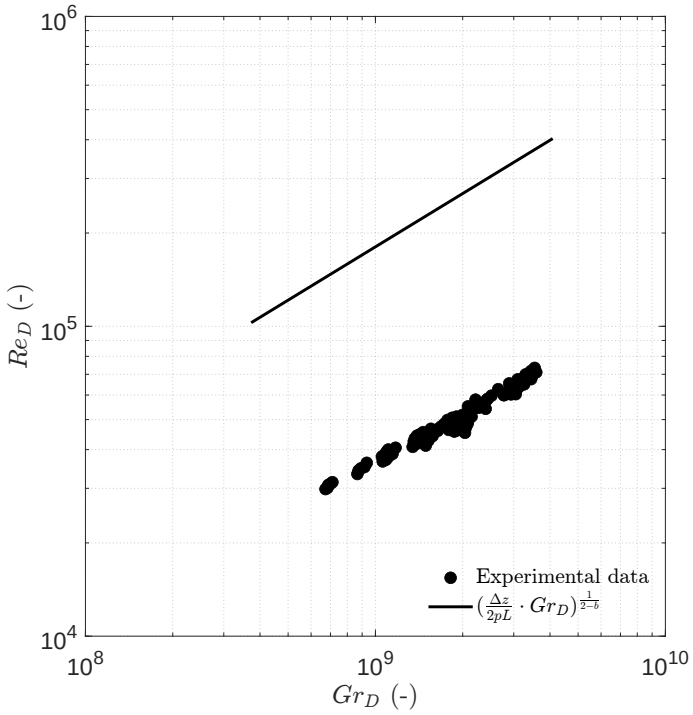

Figure 5: Re_D as function of Gr_D for experimental data in the range of operating values indicated in table 2. Prediction of equation (8) indicated in figure with solid curve.

In order to consider the independent contribution of $\dot{Q}$ in equation (6), all other terms have to attain constant values when $\dot{Q}$ is varied. Through variation of the coolant temperature, a constant thermodynamic mean state can be maintained with varying heating rates. As the measured value of $\Sigma(f_i L_i)$ is however non-constant due to variation in U, $\dot{m}_{exp}$ has to be compensated for using

$$\dot{m}_{cor,fl} = \dot{m}_{exp} \cdot \left(\frac{C_{fl}}{\Sigma(f_i L_i)_{exp}} \right)^{1/3} . \quad (10)$$

Here, $\dot{m}$ is assumed to scale with $\Sigma(f_i L_i)^{-1/3}$, following equation (6). The value of C_{fl} should be chosen such that it matches one of the values of $\Sigma(f_i L_i)$ within the considered experimental data set. As will be shown later in this work, the experimental uncertainty is the least for $\rho \geq 700$ kg m^{-3} and $p_r \geq 1.3$ within the considered range of thermodynamic states. As such, this range of thermodynamic conditions is chosen for the assessment of the individual contributions of $\dot{Q}$, Δz, and $\Sigma(f_i L_i)$. In figure 6, the expected contribution of $\dot{Q}$ is compared to corrected empirical data. Here, the measured increase in heating rate $\dot{Q} = \dot{m}_{cor,fl} \Delta h$ is used rather than the imposed electrical heating rate $\dot{Q}_{imp}$, in order to account for heating losses in the system. Close agreement is found between the predicted trend in mass flow rate and the experimental data for the considered range, hence $\dot{m}$ is assumed to scale with $\dot{Q}^{1/3}$ from this point onwards. As such, heating losses can be compensated for in investigations of data sets in which $\dot{Q}$ is to be kept constant using

$$\dot{m}_{cor,\dot{Q}} = \dot{m}_{exp} \cdot \left(\frac{\dot{Q}_{imp}}{\dot{m} \Delta h} \right)^{1/3} . \quad (11)$$

One such corrected set of empirical data is shown in figure 7. The depicted experimental data has been corrected for both variation in viscous losses, and variation in heating losses. Here, the expected change in $\dot{m}$ with variation in Δz is compared to data from experiments in which Δz is independently varied. Again, close agreement is found between theory and practice, and the source of the discrepancy in figure 5 has not yet been identified.

An investigation of the influence of thermodynamic state follows in figure 8. For the current analysis, the measured value of $\Sigma(f_i L_i)$ has been found to vary with pressure, whereas its value remains predominantly constant along each isobar. Hence, the theoretical fluid property contribution of equation (6) is multiplied with $C_{f(p_r)}$. The value of this constant is chosen as such that the theoretical curve intersects with the lowest mean temperature data point for each reduced pressure. Heating losses are compensated for using equation (11), and the corrected mass flow rate values $\dot{m}_{cor,\dot{Q}}$ are shown in the figure. The proposed theoretical contribution of thermodynamic state is found to closely and continuously describe the corrected data for any degree of sub-cooling in the considered range of parameters. Note that the size of the confidence intervals of $\dot{m}_{cor,\dot{Q}}$ varies greatly with thermodynamic state. The uncertainty in measurements of temperature and pressure is however mostly constant within the current range of experiments. As the sensitivity of enthalpy to temperature however varies with pressure, the uncertainty in enthalpy follows accordingly. This makes that the uncertainty in the determination of the fluid enthalpy used for the correction of heating losses is greatest near maxima of specific heat, hence at the pseudo-critical line at pressures in the vicinity of the critical pressure. Therefore, investigations of individual contributions of equation (6) should be performed away from the pseudo-critical curve, to reduce the uncertainty of the findings. As such, the more liquid-like, high pressure thermodynamic states are considered for these analyses, as previously elaborated on in this work.

Finally, the effect of pressure losses caused by equipment is investigated. For this, the joint pressure drop Δp_e over the flow meter and the regulating valve section is monitored. Pressure drop Δp_e is the summed value of the readings over

DOI: 10.17185/duepublico/77307

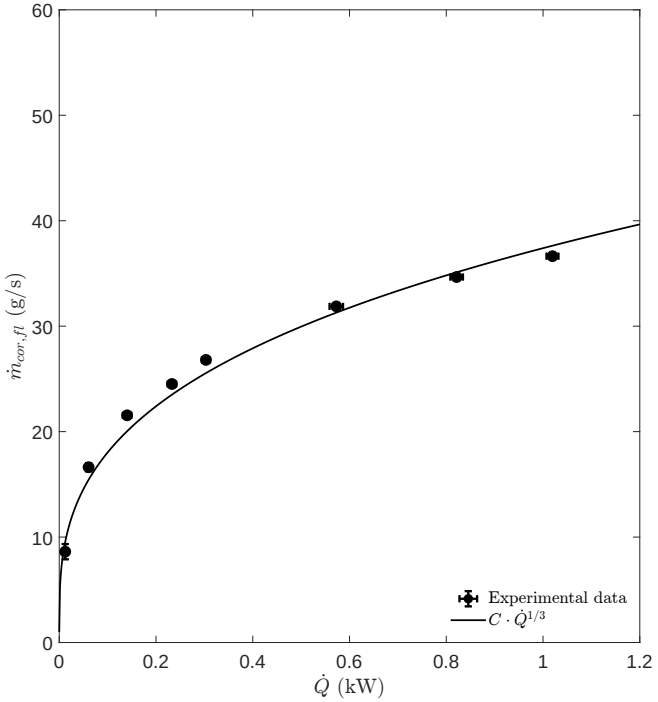

Figure 6: Variation of $\dot{m}_{\text{cor,fl}}$ with $\dot{Q} = \dot{m}_{\text{cor,fl}}\Delta h$, at $\rho_{\text{nom}} = 700\ \text{kg m}^{-3}$, $p_{\text{r}} = 1.5$, $\Delta z = 2.5$ m, with 95% confidence intervals. Constant C is chosen as such that the leftmost data point coincides with the theoretical curve.

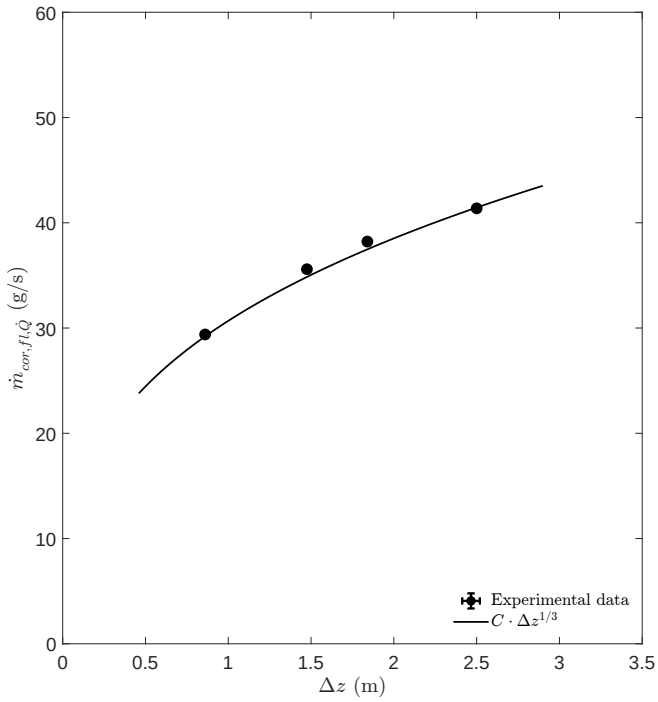

Figure 7: Variation of $\dot{m}_{\text{cor,fl},\dot{Q}}$ with Δz, at $\rho_{\text{nom}} = 700\ \text{kg m}^{-3}$, $p_{\text{r}} = 1.3$, $\dot{Q} = 800$ W, with 95% confidence intervals. Constant C is chosen as such that the rightmost data point coincides with the theoretical curve.

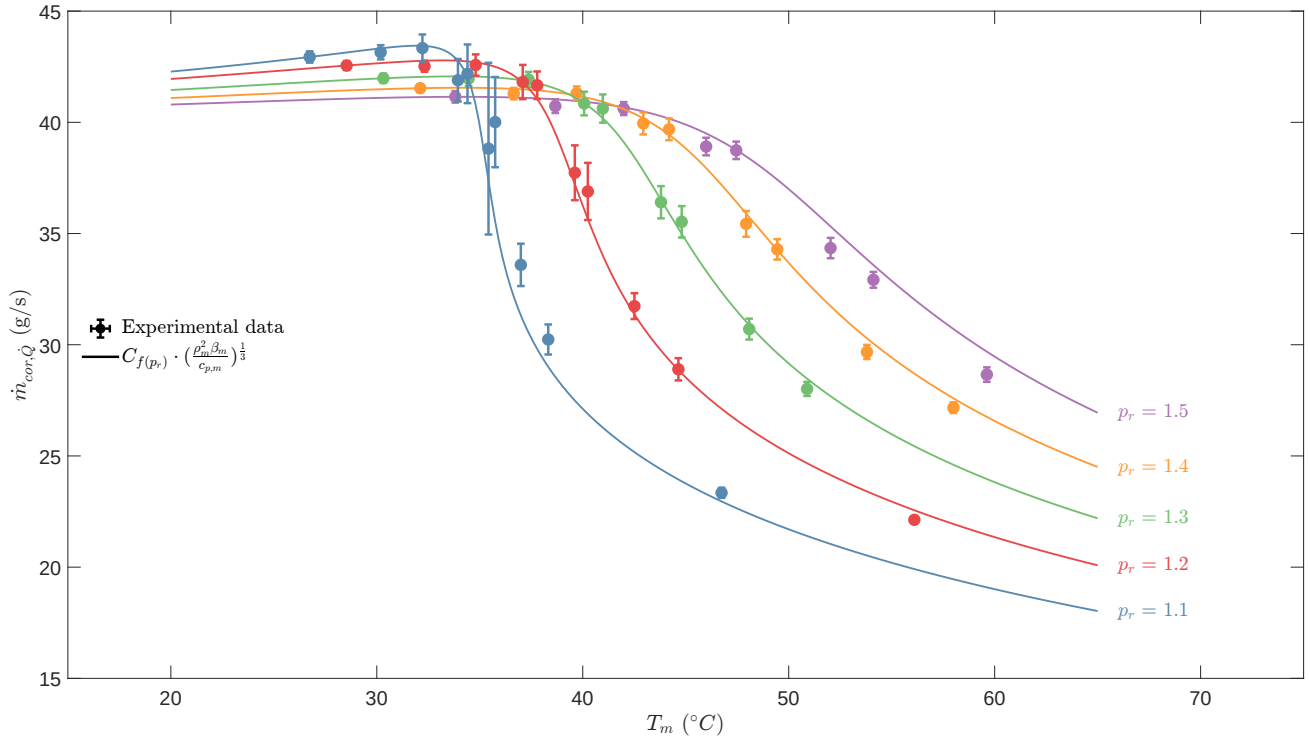

Figure 8: Variation of $\dot{m}_{\text{cor},\dot{Q}}$ with T_{m} and P_{m}, at $\Delta z = 2.5$ m, $\dot{Q} = 800$ W, with 95% confidence intervals. $C_{f(p_{\text{r}})}$ is chosen as such that the leftmost data point for each p_{r} coincides with the theoretical curve.

both differential pressure transmitters indicated with (dPT) in figure 2. Despite having different means to generate a driving force with, both natural and forced convective flows are driven by steady pressure gradients. As such, the flow in a NCL should only deviate from a developed pipe flow near heat transfer equipment where radial temperature gradients are present, and at flow obstructions. Hence, measurements of pressure losses only in obstructive equipment combined with pressure loss

DOI: 10.17185/duepublico/77307

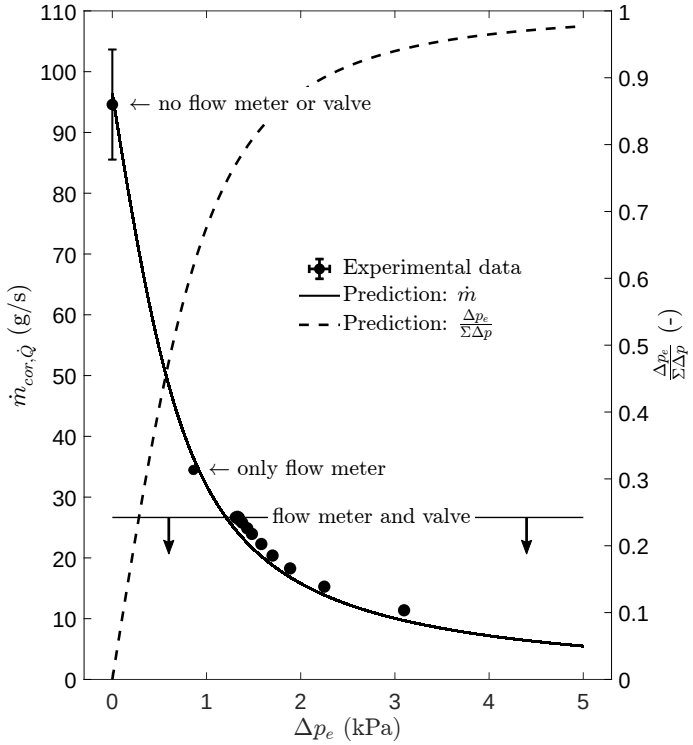

Figure 9: Left axis, full line and markers: variation of $\dot{m}_{\text{cor},\dot{Q}}$ with Δp_e, at $\rho_\text{nom} = 730$ kg m^{-3}, $p_\text{r} = 1.1$, $\Delta z = 2.5$ m, $\dot{Q} = 400$ W, with 95% confidence intervals. Predictive curve found by varying the equipment loss term $(fL)_\text{e}$ in equation (6), and iteratively solving for $\dot{m}$. The leftmost data point has not been corrected to take heating losses into account. Right axis, dotted line: Δp_e as a fraction of the estimated total loop pressure loss $\Sigma \Delta p$.

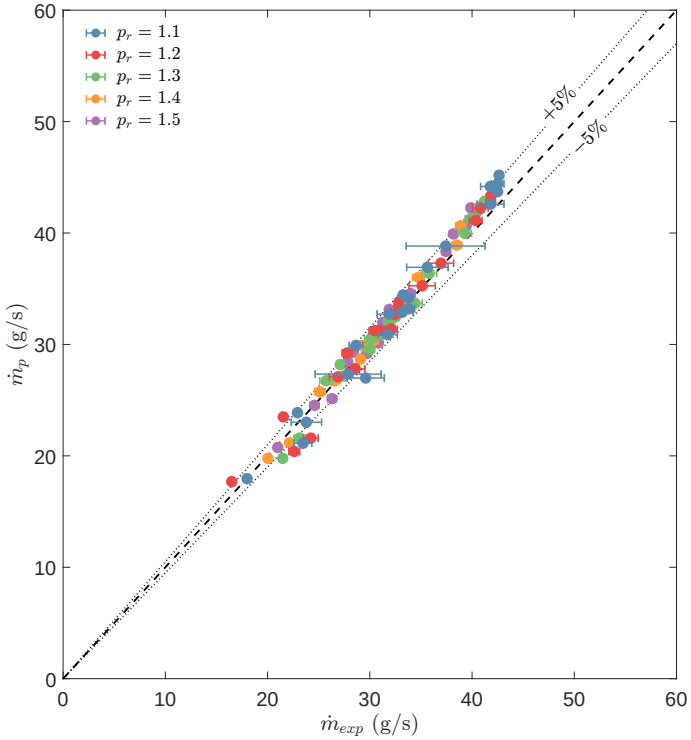

Figure 10: Steady state prediction error with inclusion of measured Δp_e into equation (6), at $\Delta z = 2.5$ m, $\dot{Q} = 400$ W $\vee$ $\dot{Q} = 800$ W, with 95% confidence intervals.

correlations based on ideal and developed pipe flows should suffice in reconstructing the NCL's sensitivity to pressure losses.

Figure 9 shows the loop mass flow rate as a function of the experimental values of Δp_e, and the relative magnitude of Δp_e with respect to the total viscous pressure losses in the system. The regulating valve is present in all but two data points of the current analysis, for which it is removed from the supercritical NCL. In the leftmost data point in the figure, both the valve and the mass flow meter are removed from the experimental facility. Here, the mass flow rate is estimated from the imposed heating rate and the measured enthalpy increase over the heater, i.e. $\dot{m}_\text{exp} = \dot{Q}_\text{imp}/(h_\text{h,exp} - h_\text{c,exp})$. As heating losses cannot be reliably estimated for this data point, they are not compensated for. The predictive curve is obtained by adding an equipment loss term $(fL)_\text{e} = (\Delta p_\text{e} D)/(2\rho_\text{c} U_\text{c}^2)$ in the viscous loss term in equation (6). For each value of Δp_e, the distribution of the viscous losses in the system has to be iteratively solved for. As such, the presented theoretical curve in figure 9 is state- and configuration dependent and therewith only applicable to the current analysis.

The theoretical curve is found to closely resemble the experimental data. The value of the predictive curve at a zero value of Δp_e corresponds to the expected mass flow rate in case no equipment losses are assumed. For this point, the total loop pressure loss is solely predicted using the turbulent Blasius viscous loss constants specified previously in this section. Whilst this modeling assumption is likely to be accurate for the majority of the loop, the relatively large uncertainty in the unobstructed and leftmost data point makes that no definitive claims regarding the validity of the modeling choice can be made. Furthermore, a comparison of the two leftmost points in the figure shows that a threefold decrease in mass flow rate is the direct consequence of the inclusion of a flow meter in the experimental loop. The difference in mass flow rate is of similar magnitude as the shift in figure 5, in which equipment pressure losses were not taken into account. As can be seen from figure 9, the losses in the flow meter alone are estimated to exceed the regular viscous losses in the loop.

Figure 10 shows the error in the prediction of the experimental steady state mass flow rate $\dot{m}_\text{exp}$, if the measured Δp_e is included in the viscous loss term of equation (6). As shown in the figure, close agreement is found with the predicted mass flow rate $\dot{m}_\text{p}$ for the majority of the data.

Albeit moderately, the value of $\dot{m}_\text{exp}$ is systematically over-predicted for the more liquid-like data points of the considered range, shown mostly in the top half of figure 10. A possible cause for the above is an under-prediction of the viscous losses in the flow in the vicinity of the heat transfer equipment of the setup. As qualitatively described in the work of Wahl et al. [17], the alignment of the direction of both forced- and natural convection can result in near-wall velocities that are greater than in an adiabatic setting. For flows of supercritical

DOI: 10.17185/duepublico/77307

media, this is the case for downward cooled and upward heated pipe flows. As such alignment is present in both heat transfer configurations of the investigated loop for the preferential flow direction, enhanced buoyancy-aided shear is expected in- and directly downstream of the cooler and heater. From the correlations presented in the review of Fang et al. [18], it follows that the greatest degrees of shear enhancement can be found for more liquid-like states beyond the critical point. As these additional viscous losses are not measured and hence not taken into account for the determination of $\dot{m}_\mathrm{p}$ in figure 10, the true steady state is likely over-predicted.

For all the considered experimental data points of this work, the total loop viscous losses are dominated by the equipment losses of a single Coriolis transmitter. The associated loss of flow rate is expected to be even more prevalent in facilities with less simple geometries, in which the flow is forced through a greater amount of instruments, or past series of turbine blades. Hence, the a priori characterization of the equipment minor losses is essential for an accurate prediction of the steady mass flow rate of supercritical NCLs, which are generally inflexible to changes in maximum heat throughput. Without the proper portrayal of such losses, an empirical fit based on equation (8) yields little insights for the development of future circulation loops. Additionally, equation (6) will only serve as a qualitative measure of the evolution of $\dot{m}$ with thermodynamic state, Δz and $\dot{Q}$ from some configuration specific steady state value.

CONCLUSIONS

The steady state behavior of a natural circulation loop that employs thermodynamically supercritical carbon dioxide was experimentally investigated in this work. The experiments were conducted using a novel facility at the Process & Energy laboratory of the Delft University of Technology. Distinct empirical data points were obtained by varying the system's filling mass, its heating rate, and the temperature of the coolant. The experimental data was compared to a newly proposed generalized equation for the prediction of the steady state mass flow rate of supercritical NCLs. Whereas the effects of changes in heating rate, differential heating height, and state were shown to be accurately captured in isolated experiments, the experimental mass flow rate was significantly over-predicted. The over-prediction was attributed to the viscous losses in the instrumentation, which can significantly limit the flow rates in these systems in which the driving forces are generally of moderate magnitudes. Therefore, an in-advance assessment of equipment losses is required for the accurate prediction of yet to be developed supercritical NCL systems.

ACKNOWLEDGEMENTS

This work was funded by the European Research Council grant no. ERC-2019-CoG-864660, Critical.

REFERENCES

[1] S. Sadhu, M. Ramgopal, and S. Bhattacharyya, "Steady-state analysis of a high-temperature natural circulation loop based on water-cooled supercritical co2," *Journal of Heat Transfer*, vol. 140, no. 6, 2018.

[2] P. K. Jain and R. Uddin, "Numerical analysis of supercritical flow instabilities in a natural circulation loop," *Nuclear Engineering and Design*, vol. 238, no. 8, pp. 1947–1957, 2008.

[3] M. Sharma, D. Pilkhwal, P. Vijayan, D. Saha, and R. Sinha, "Steady state and linear stability analysis of a supercritical water natural circulation loop," *Nuclear Engineering and Design*, vol. 240, no. 3, pp. 588–597, 2010.

[4] A. S. Pegallapati, P. Banoth, and R. Maddali, "Dynamic model of supercritical co2 based natural circulation loops with fixed charge," *Applied Thermal Engineering*, vol. 169, p. 114 906, 2020.

NOMENCLATURE

Symbol	Property	Unit
	Symbols	
A_cs	Cross sectional area ($\pi D^2/4$)	m^2
A_p	Pipe wall area (πDL)	m^2
b	Constant in eq (9)	-
c_p	Specific heat	$\mathrm{J\,kg^{-1}K^{-1}}$
C_fl	Constant in eq. (10)	-
D	Internal pipe diameter	m
f	Fanning friction factor	-
F	Force	N
g	Gravitational acceleration	$\mathrm{m\,s^{-2}}$
Gr_D	Grashof number, eq (7)	-
h	Specific enthalpy	$\mathrm{J\,kg^{-1}}$
H	Total loop height	m
L, L_i	Loop length, section length	m
$\dot{m}$	Mass flow rate	$\mathrm{kg\,s^{-1}}$
p	Constant in eq (9)	-
P	Pressure (absolute)	Pa
$\dot{Q}$	Heating rate	W
s	Streamwise coordinate	m
T	Temperature	K
U	Streamwise velocity component	$\mathrm{m\,s^{-1}}$
Δz	Vertical point-source heater-cooler distance	m

Symbol	Property	Unit
	Greek symbols	
β	Volumetric expansivity	$\mathrm{K^{-1}}$
γ	Directional coefficient in eq (2)	-
μ	Dynamic viscosity	Pa s
ρ	Density	$\mathrm{kg\,m^{-3}}$
	Subscripts	
c	Value taken at temperature and pressure of cold leg	
cor,$\dot{Q}$	Corrected for variation in $\dot{Q}$	
cor,fl	Corrected for variation in $\Sigma(f_\mathrm{i}L_\mathrm{i})$	
crit	Value at critical point	
D	Pipe inner diameter as characteristic lengthscale	
e	Value at specified equipment	
exp	Experimental value	
h	Value taken at temperature and pressure of hot leg	
imp	Imposed value	
m	Value taken at loop mean temperature and pressure	
nom	Nominal/intended value	
p	Predicted value	
r	Reduced value, with respect to value at critical point	

DOI: 10.17185/duepublico/77307

[5] M. K. Sarkar and D. N. Basu, "Influence of geometric parameters on thermalhydraulic characteristics of supercritical co2 in natural circulation loop," *Nuclear Engineering and Design*, vol. 324, pp. 402–415, 2017.

[6] H. Tokanai, Y. Ohtomo, H. Horiguchi, E. Harada, and M. Kuriyama, "Heat transfer of supercritical co2 flow in natural convection circulation system," *Heat transfer engineering*, vol. 31, no. 9, pp. 750–756, 2010.

[7] G. Liu, Y. Huang, J. Wang, F. Lv, and L. K. Leung, "Experiments on the basic behavior of supercritical co2 natural circulation," *Nuclear Engineering and Design*, vol. 300, pp. 376–383, 2016.

[8] L. Chen, B.-L. Deng, and X.-R. Zhang, "Experimental investigation of co2 thermosyphon flow and heat transfer in the supercritical region," *International Journal of Heat and Mass Transfer*, vol. 64, pp. 202–211, 2013.

[9] S. Sadhu, M. Ramgopal, and S. Bhattacharyya, "Experimental studies on an air-cooled natural circulation loop based on supercritical carbon dioxide–part a: Steady state operation," *Applied Thermal Engineering*, vol. 133, pp. 809–818, 2018.

[10] S. Yoshikawa, R. L. Smith Jr, H. Inomata, Y. Matsumura, and K. Arai, "Performance of a natural convection circulation system for supercritical fluids," *The Journal of supercritical fluids*, vol. 36, no. 1, pp. 70–80, 2005.

[11] B. Swapnalee, P. Vijayan, M. Sharma, and D. Pilkhwal, "Steady state flow and static instability of supercritical natural circulation loops," *Nuclear Engineering and Design*, vol. 245, pp. 99–112, 2012.

[12] P. Vijayan and H. Austregesilo, "Scaling laws for single-phase natural circulation loops," *Nuclear Engineering and Design*, vol. 152, no. 1-3, pp. 331–347, 1994.

[13] P. Vijayan, "Experimental observations on the general trends of the steady state and stability behaviour of single-phase natural circulation loops," *Nuclear engineering and design*, vol. 215, no. 1-2, pp. 139–152, 2002.

[14] W. Ambrosini and M. Sharabi, "Dimensionless parameters in stability analysis of heated channels with fluids at supercritical pressures," *Nuclear Engineering and Design*, vol. 238, no. 8, pp. 1917–1929, 2008.

[15] G. Liu, Y. Huang, and J. Wang, "A new theoretical model of steady-state characteristics of supercritical carbon dioxide natural circulation," *Energy*, vol. 189, p. 116 323, 2019.

[16] L. Ansaloni, B. Alcock, and T. A. Peters, "Effects of co2 on polymeric materials in the co2 transport chain: A review," *International Journal of Greenhouse Gas Control*, vol. 94, p. 102 930, 2020.

[17] A. Wahl, R. Mertz, E. Laurien, and J. Starflinger, "Heat transfer deterioration in vertical sco2 cooling in 3 mm tube," *Energy*, p. 124 240, 2022.

[18] X. Fang, L. Xu, Y. Chen, and W. Chen, "Correlations for friction factor of turbulent pipe flow under supercritical pressure: Review and a new correlation," *Progress in Nuclear Energy*, vol. 118, p. 103 085, 2020.

DOI: 10.17185/duepublico/77307